Digest Journal of Nanomaterials and Biostructures Vol. 18, No. 3, July - September 2023, p. 1039 - 1049

Characterization of silver oxide thin films with thickness variation prepared by thermal evaporation method

F. A. Jasim[a*], Z. S. A. Mosa[b], N. F. Habubi[c], Y. H. Kadhim[d], S. S. Chiad[e]
[a]*Department of Physics, College of Science, Mustansiriyah University, Iraq*
[b] *Department of Pharmacy, Al-Manara College for Medical Science, Iraq.*
[c]*Department of Radiation and Sonar Technologies, AlnukhbaUniversity College, Iraq*
[d]*Department of Optics Techniques, Al-Mustaqbal University College, Babylon, Iraq.*
[e]*Department of Physics, College of Education, Mustansiriyah University, Iraq.*

Thermal evaporation technique has been used to produce silver oxide (AgO). The findings demonstrate that the crystal quality of the AgO film was dominated by the thin and sharp peaks at (111) plans. Atomic Force Microscopy (AFM) confirm that the distribution grains size appears nanostructure and homogeneous in all films. RMS decreased from 6.84 nm to 2.17 nm with thicknesses 200 nm. The surface roughness decreased from 7.82 nm to 3.22 nm. The distribution of grains size appears nanostructured and homogeneous in all films, and a slight decrease in average particle size. The surface displayed that the roughness decreased with the increase in thicknesses. The spectrum fluctuation of their optical constants has been calculated using transmittance and absorption data. In the visible region of the wavelength, all films have a high absorption coefficient with a value of 10^4 (cm^{-1}). According to the optical measurements, the films have a band gap between 1.73 and 1.61 eV. The Extinction coefficient and refractive index drop as film thickness rises.

(Received May 29, 2023; Accepted August 28, 2023)

Keywords: Silver oxide films, Thermal evaporation, X-ray diffraction, AFM.

1. Introduction

Due to their unusual optical characteristics, thin silver films have received much attention [1, 2]. Numerous optical technologies, including solar cells and light-emitting diodes, as well as ways to enhance the characteristics of organic semiconductor materials and introduce novel metamaterials, have found a use for them [3, 4]. According to studies, silver oxide films have a band gap that ranges from 1.2 to 3.4 eV, making them useful as sensors for gas detection and photovoltaic materials [5, 6]. The aggregation of grains during the grown of thin films is known to be controlled by the deposition circumstances, including the rate of deposition, vacuum pressure, and type and temperature of the substrate. [7,8]. Many methods were employed to grow AgO like, PLD [9]. RF, DC sputtering [10,11], chemical synthesis [12], vapor-liquid-solid process [13], CBD [14]. Spray pyrolysis method [15], and Thermal Evaporation [16-19]. One of the first methods for depositing thin films is thermal evaporation, which is still commonly employed in research labs and industrial settings to deposit metals and metal alloys. The production of thin films of semiconducting materials and alloys has already been done using this method. The thickness Effect on the optical characteristics of thin silver coatings produced by thermal evaporation is the subject of the current study.

2. Experimental

For the deposition of Ag thin films, glass slides were employed as the substrate material. They were cut using a steel cutter tool into squares measuring (1.51.5) cm^2, which were in line with the size of the substrate holder. To get rid of the protein compounds and contaminants on the glass slides' surface, a diluted chemical detergent solution was used to clean them. Using a coating unit at a vacuum of around (210-5) Torr. Ag with three masses of 1.00g, 1.15g, and 1.29 g was

* Corresponding author: Farah.A.J@uomustansiriyah.edu.iq
https://doi.org/10.15251/DJNB.2023.183.1039

deposited using the thermal evaporation method. All samples had identical deposition times of 1 minute, and their evaporation rates were 23.5 nm/min. At a distance of around 18 cm, the well-cleaned glass base was positioned directly above the source. The film thickness (100, 150, and 200 nm) was determined using the interference technique. With the aid of Xray diffractometer (Angstrom AA 3000), Ag thin films were examined independently. Atomic force microscopy (AFM) and optical transmittance spectra for thin films that had already been deposited were captured using a UV-visible shimadzu twin-beam spectrophotometer that operated in the 300-900 nm wavelength range.

3. Results and discussions

From Figure 1, four peaks at 2θ = 32.03°, 37.24°, 54.71° and 63.46° of silver-coated films with polycrystalline F.C.C structure. The corresponding planes are (200), (111), (202) and (311. The peak obtained for the thin film at 2θ = 37.24° has a considerably higher intensity, indicating that the (111) orientation is the preferred direction for growth. In addition, it was compared to JCPDS card No. (43-1038). The cleanliness of the coated films is also evident in Figure 1. [19]. These results agree with Alhasan et al [20].

The crystallite size(D) were determined employing Scherrer formula [21-23]:

$$D = \frac{0.9\lambda}{\beta cos\theta} \quad (1)$$

where λ is the X-ray wavelength, β is FWHM, and 2θ is the diffraction angle in degrees. The computed D for thicknesses of 100 nm, 150 nm, and 200 nm are 13.52 nm, 13.97 nm, and 14.70 nm, respectively. It was found that when thickness rose, the average crystal size increased. [20].

The quantity of defects present in the grown samples is calculated using the following equation, and the dislocation density is employed. [24-26].

$$\delta = \frac{1}{D^2} \quad (2)$$

The lattice strain (ε) has been determined by using the tangent formula [27-29]:

$$\varepsilon = \frac{\beta cos\theta}{4\pi} \quad (3)$$

Table 1 summarizes (D), (δ) and (ε) of AgO thin films grown by using various thicknesses. The acquired structural characteristics are shown in Table 1, with the strain value decreasing with increasing thicknesses. Figure (2) shows thicknesses vs FWHM, D.

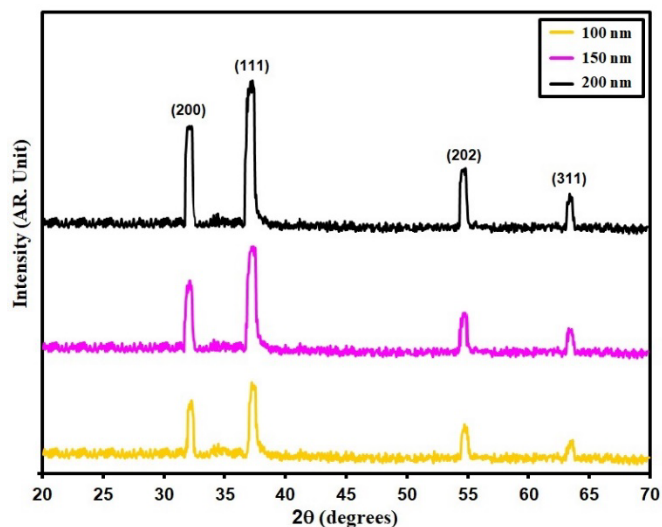

Fig.1. XRD of AgO films.

Table 1. shows the XRD parameters calculated for AgO films with different thicknesses.

Thickness (nm)	2 θ (º)	(hkl) Plane	FWHM (º)	Optical bandgap (eV)	Grain size (nm)	Dislocations density ($\times 10^{14}$) (lines/m^2)	Strain ($\times 10^{-4}$)
100	37.24	111	0.62	1.73	13.52	54.70	25.63
150	37.20	111	0.60	1.68	13.97	51.23	24.80
200	37.15	111	0.57	1.61	14.70	46.22	23.57

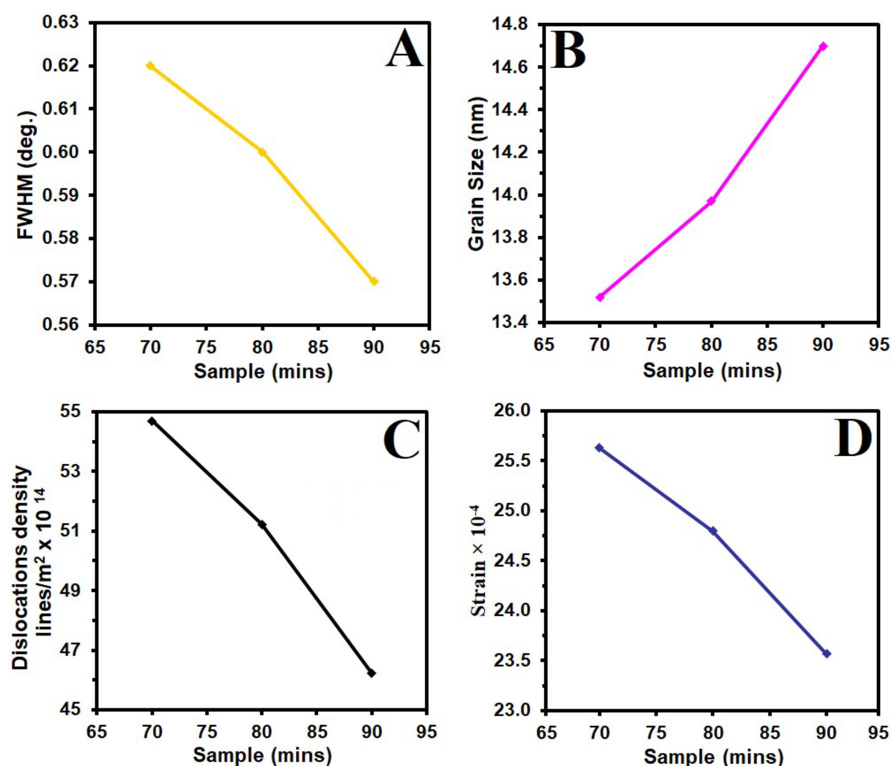

Fig.2.a) FWHM b) D c) δ and d) ε parameters of the grown films.

4. Topography surface analysis

By using AFM analysis, the films' surface morphology was investigated. All films had a scan area of (2 x 2) mm. Figure 3 (A_1, A_2, and A_3) displays three-dimensional AFM pictures of the silver films as they were deposited on the glass substrate. Smaller particles have developed on the surface of the substrate, and the pyramidal shape is visible. The distribution grains size appears nanostructure and homogeneous in all films and slight decrease in average particle size. The surface displayed that the roughness decreased with the increased thicknesses. The AgO crystallites developed substantially on the grain morphology are represented by the bright spot on the film's surface [20]. Table 2 lists the variables, including average roughness (Ra), average particle size, and root mean square roughness (RMS). With thicknesses of 200 nm, it was seen that the root mean square (RMS) roughness assessed from AFM images dropped from 6.84 nm to 2.17 nm. Fig. 3 illustrates spherical nanoparticles of uniform distribution constitute the surface of the AgO thicknesses (100, 150 and 200) nm films. Introduction These particles have an extremely high particle density per unit area and a very narrow size distribution. This demonstrates the film's excellent crystalline quality. As the thickness was increased, the granules grew smaller [31]. This outcome agrees with the XRD data. As shown in Table 2, the AFM measurement of grain size is larger than the XRD measurement. AFM provides the grain size according to the distances between the discernible grain boundaries.

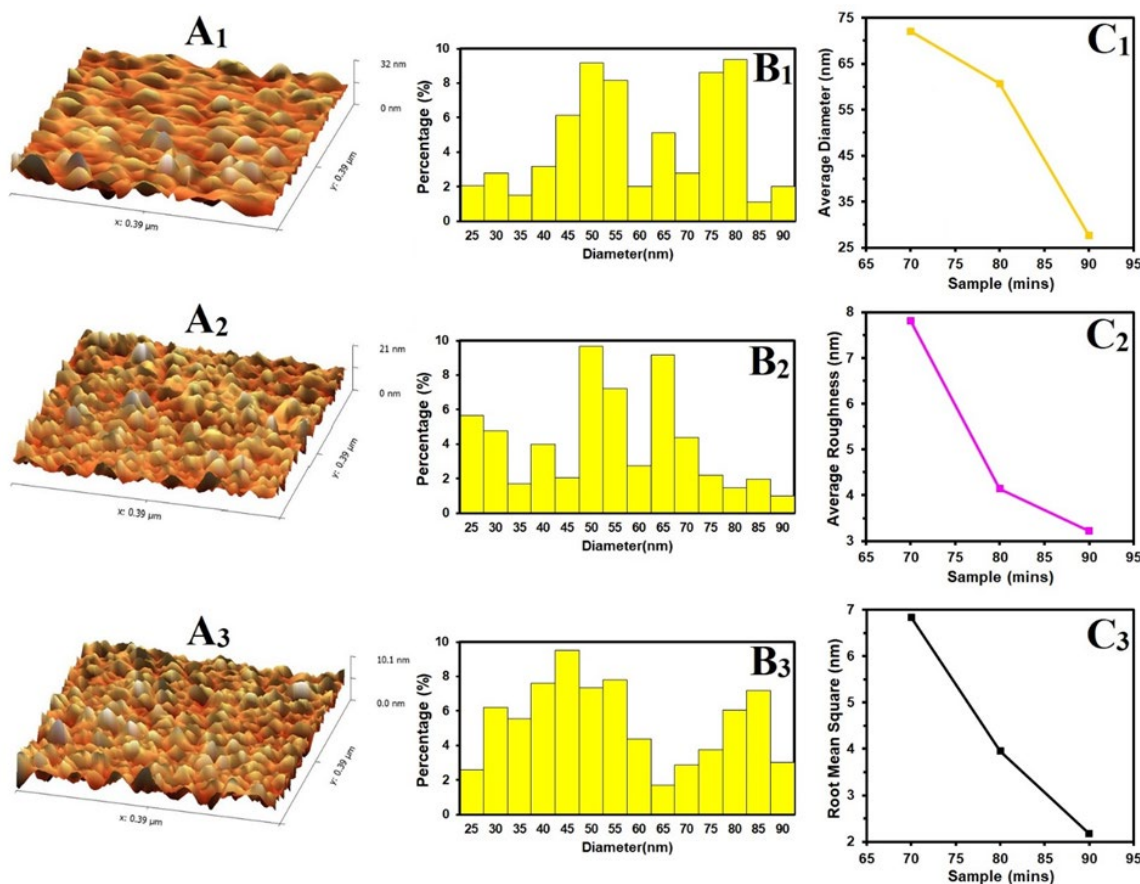

Fig.3: Atomic force microscope images (A1- A1), granularly distributed (B1- B3) and diversity of AFM parameters against doping (C1 -C3).

Table 2. AFM Parameters of AgO films with different thicknesses

Thickness (nm)	Average Particle size nm	R_a (nm)	R. M. S. (nm)
100	72.0	7.82	6.84
150	60.7	4.14	3.95
200	27.6	3.22	2.17

5. Optical properties analysis

Figure 5 illustrates the films' transmittance (T%) and absorption spectra. All films exhibit between 90 and 96 percent transmittance in the visible spectrum. The films also show increased transmittance values in the long wavelength area of the spectra. The transmittance value quickly rose from the (400-900 nm) range. This might be due to intergranular porosities found in the films in AFM pictures. Undoped film has greater T%, and T% declines with thickness. [32].

The measured absorbance (A) of the film is related to transmittance (T) by [33-35]:

$$A = \log\left(\frac{1}{T}\right) = \left(\frac{I}{I_o}\right) \quad (4)$$

where the incident light is (Io), and the transmitted light is (I). UV-VIS spectrophotometer measurements were used to record the optical absorption spectrum (absorbance as a function of wavelength). The wavelength-dependent absorbance curve is shown in Figure 4. The thickness of the formed AgO thin film affects its absorption, and optical absorption spectra between 300 and 900 nm were obtained. Figure (4) shows that for photons with a wavelength between 300 and 90 nm, AgO thin film with a thickness of 100 nm had the lowest absorbance and AgO thin film with a thickness of 200 nm had the greatest. This was due to the rise in film thickness. [36].

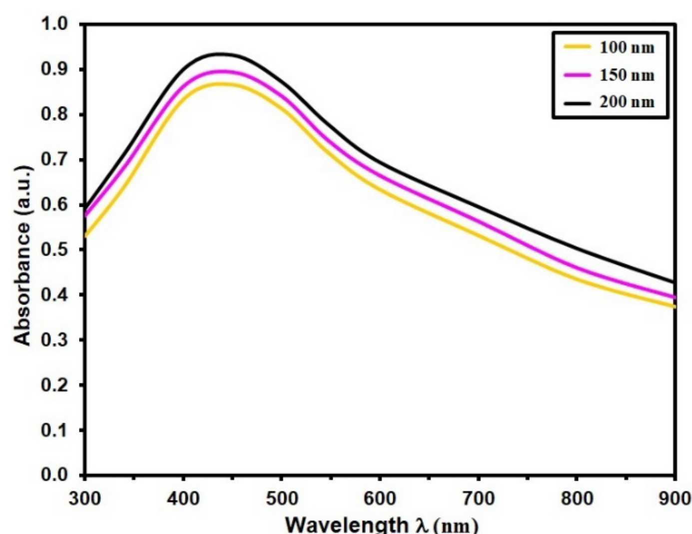

Fig. 4: Absorbance of AgO thin films.

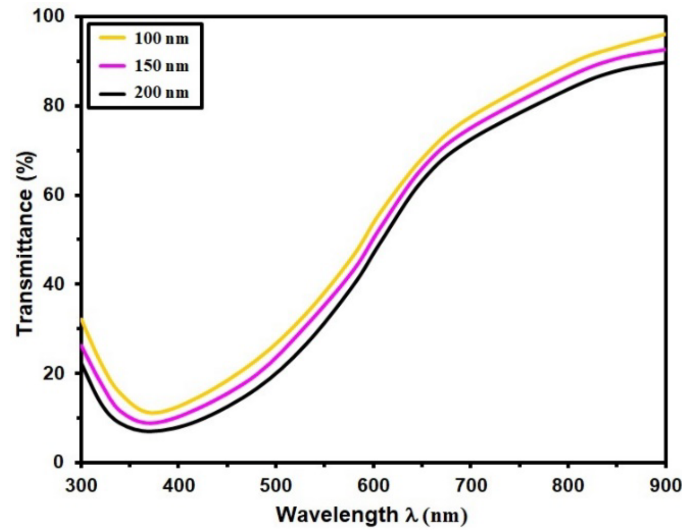

Fig. 5: Transmittance of AgO films.

Equation 5 is used to compute the absorption coefficient α [37-39]:

$$\alpha = \frac{\ln{(1/T)}}{d} \tag{5}$$

where d is the film's thickness. Figure 6 shows the change in. In the visible region of the wavelength, all films exhibit a high αwith value of 10^4 (cm^{-1}), indicating a straight transition. [19]. αincreases with increasing thickness.

The bandgap energy (E_g) was calculated via Tauc's relation [40-42]:

$$(\alpha h\nu) = A(h\nu - E_g)^n \tag{6}$$

where A is a constant, hν is the photon's energy, and n depends on the kind of transition.

Depending on whether they are permitted or disallowed, respectively, n is 1/2. The measured values for thicknesses of 100 nm, 150 nm, and 200 nm are 1.73 eV, 1.68 eV, and 1.61 eV, respectively (Figure 7). As the thickness rises, the band gap somewhat narrows.

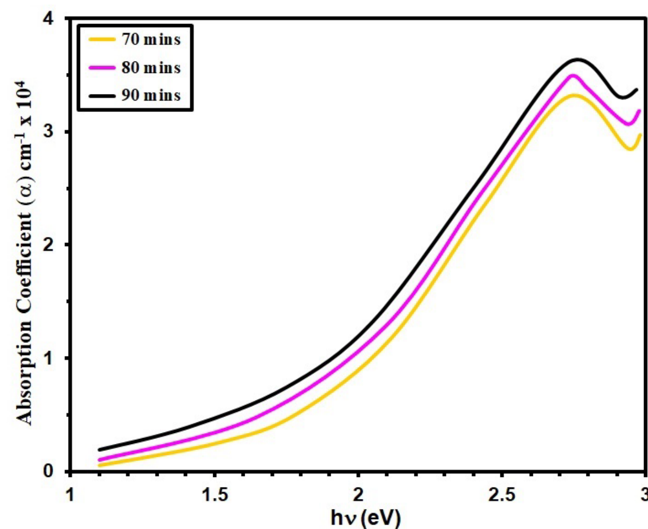

Fig. 6: α Vs hν of AgO films.

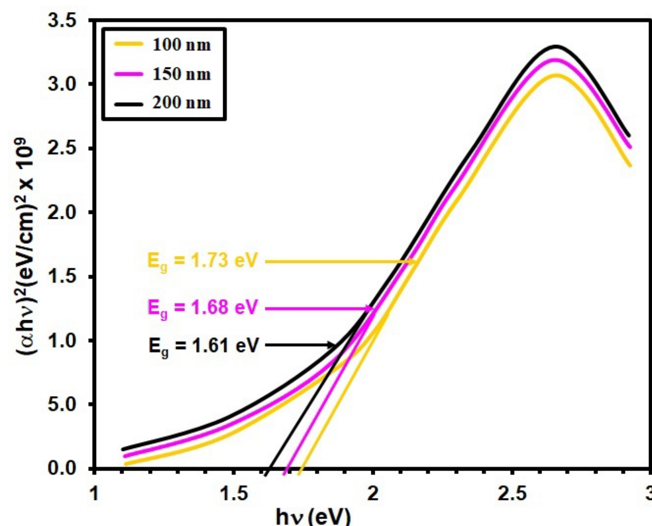

Fig. 7: (αhν)2 against hν AgO thin films.

The extinction coefficient of the films is calculated from the equation [43-45]:

$$k = \frac{\alpha\lambda}{4\pi} \tag{7}$$

where α is the absorption coefficient.

According to Fig. 8, the k value decreased with wavelength starting at 440 nm in the UV-visible area and became saturated in the 600-900 nm VIS-infrared region. The value of k is between 0.14 and 0.48, with the greater value occurring at about 440 nm, where it progressively rises with decreasing thicknesses of 200 nm.
The refractive index analyses the material's electrical and optical characteristics. It is connected to the local field of the material and the electronic polarization of ions, with 1.61 eV for thicknesses of 100 nm, 150 nm, and 200 nm, respectively (Figure 7). As the thickness rises, the band gap somewhat narrows. One way to calculate anything is to use the formula k = extinction coefficient or absorption index, R = reflectance, and n = refractive index. It is commonly known that films' refraction depends on how incident light interacts with the substance and that it rises as there are more particles per unit area of light. Utilizing the reflectance (R) spectra, one may calculate the refractive index (n) [46,47]:

$$R = \left(\frac{n-1}{n+1}\right)^2 \tag{8}$$

The formula was used to calculate the refractive index (n) of an AgO thin layer. [48]

$$n = \frac{1+\sqrt{R}}{1-\sqrt{R}} \tag{9}$$

where k is the extinction coefficient or absorption index, R is the reflectance, and n is the refractive index It is well known that the refractivity of films relies on how incident light interacts with the material, and that the refractivity of films increases when there are many particles per unit area of light. Fig.9. shows the maximum value of *n* lies in the region 450-550 nm and *n* decreased with increasing thicknesses. This may indicate the increase in the film's density after increasing thicknesses and *n* fell with increasing thicknesses [49].

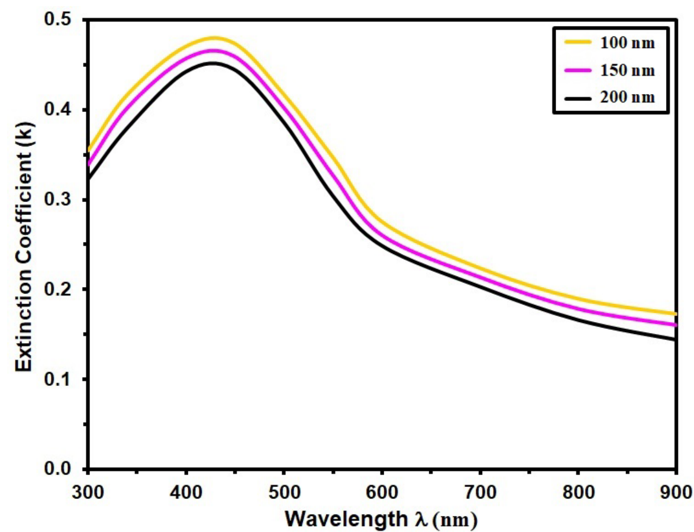

Fig. 8: Extinction coefficient (k) of AgO films.

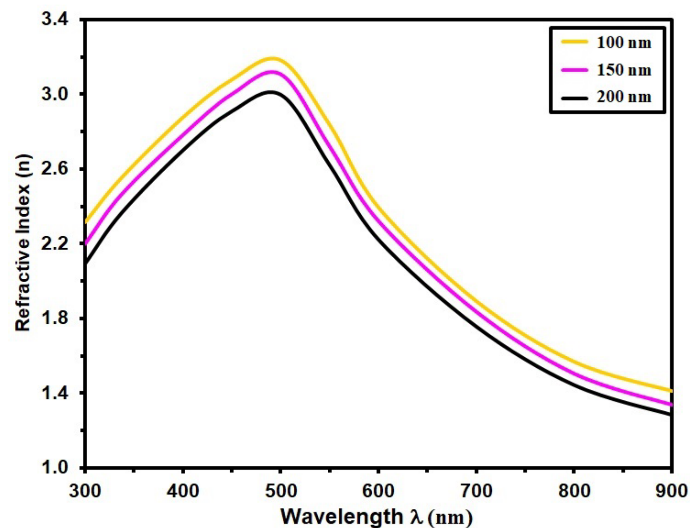

Fig. 9. Refractive Index of thin films (Ag) these deposited on substrate (glass).

6. Conclusion

Silver oxide thin films are grown using thermal evaporation (homemade). Their structural, morphology and optical properties were investigated using XRD, AFM and UV-Vis. The average grain sizes are 13.52 nm, 13.97 nm and 14.70 nm for thicknesses of (100), 150 and 200) nm, respectively. As layer thickness increases, strain and dislocation density become less significant. Spectrophotometer and atomic force microscopy. With thicknesses of 200 nm, the root mean square (RMS) roughness measured from AFM images dropped from 6.84 nm to 2.17 nm. The absorption coefficient increased slightly as the film thickness increased, while the transmittance, band gap, refractive index and Extinction coefficient decreased as film thickness increased.

Acknowledgements

The authors would like to thank Mustansiriyah University and Alnukhba University College for propped this work.

References

[1] N. R. C. Raju, K. J. Kumar and A. Subrahmanyam, J. Phys. D: Appl. Phys. 42, 135411 (2009); https://doi.org/10.1088/0022-3727/42/13/135411
[2] A.R. Bushroa, R.G. Rahbar, H.H. Masjuki and M.R. Muhamad, Vacuum, 86, 1107 (2012); https://doi.org/10.1016/j.vacuum.2011.10.011
[3] K. Sivalingam, P. Shankar, G.K. Mani and J.B.B. Rayappan; Mater. Lett., 134, 47 (2014); https://doi.org/10.1016/j.matlet.2014.07.019
[4] L. A. Peyser, A. E. Vinson, A. P. Bartko and R. M. Dickson; Science, 291, 103 (2001); https://doi.org/10.1126/science.291.5501.103
[5] X. Zhang, S. Ma, F. Yang, Q. Zhao, F. Li and L. Jing; Ceram. Int., 39, 7993 (2013); https://doi.org/10.1016/j.ceramint.2013.03.066
[6] M. Fujimaki, K. Awazu and J. Tominaga; J. Appl. Phys., 100, 074303 (2006); https://doi.org/10.1063/1.2354329
[7] Z.N. Kayani, T. Afzal, S. Riaz and S. Naseem; J. Alloys Compd., 606, 177 (2014); https://doi.org/10.1016/j.jallcom.2014.04.039
[8] F. Fang, Q. Li and J. K. Shang; Surface & Coatings Technology, 205, 2919 (2011); https://doi.org/10.1016/j.surfcoat.2010.10.068
[9] B J Alwan, L G Subhi, A N Abd, IOP Conf. Series: Materials Science and Engineering, 454, 012101(2018);
https://doi.org/10.1088/1757-899X/454/1/012101
[10] U. K. Barik, S. Srinivasan, C. L. Nagendra and A Subrahmanyam, Thin Solid Films, 429,129 (2003);
https://doi.org/10.1016/S0040-6090(03)00064-6
[11] Y. C. Her, Y. C. Lan, W. C. Hsu and S. Y. Tsai; Japan. J. Appl. Phys., 43, 267 (2004);
https://doi.org/10.1143/JJAP.43.267
[12] B. J. Murray, Q. Li, J. T. Newberg, E. J. Menke, J. C. Hemminger and R. M. Penner, Nano Letters, 5 (11), 2319-2324 (2005); http://dx.doi.org/10.1021/nl051834o
[13] Marwa A Dawood, Makram A Fakhri, Farah G Khalid, Materials Science and Engineering, 454 (1) 012161 (2018); http://dx.doi.org/10.1088/1757-899X/454/1/012161
[14] M. K. Abood, M Halim A Wahid, E. T. Salim, Jehan Admon, the European Physical Journal Conferences 162(12), 01058 (2017); https://doi.org/10.1051/epjconf/201716201058
[15] M. F. Al-kuhaili; J. Phys. D: Appl. Phys., 40, 2847 (2007);
https://doi.org/10.1088/0022-3727/40/9/027
[16] S. Singh, A. Sharma, P. Kumar, R. Thangavel, Journal of Materials Science: Materials in Electronics, 29 (14), 11967-11974 (2018);
https://doi.org/10.1007/s10854-018-9476-0.
[17] R. Bharti, V. Sharma, A. Kumar, P. Saini, " Materials Today: Proceedings, 5 (2) 5296-5301 (2018); https://doi.org/10.1016/j.matpr.2017.12.228.
[18] D. H. Kim, S. H. Ahn, K. H. Kim, Journal of Applied Physics, 119(15), 155305 (2016); https://doi.org/10.1063/1.4947034
[19] Khomane, R. B., et al., Structural and optical properties of silver oxide thin films prepared by thermal evaporation. Materials Science in Semiconductor Processing, 81, 81-86 (2018); https://doi.org/10.1016/j.mssp.2018.02.019
[20] C. Guillen and J. Herrero; Vacuum, 84, 924 (2010); https://doi.org/10.1016/j.vacuum.2009.12.015

[21] E. S. Hassan, A.K. Elttayef, S.. Mostafa, M. H. Salim, S.S. Chiad, Journal of Materials Science: Materials in Electronics, 30 (17), 15943-15951, (2019); https://doi.1007/s10854-019-01954-1
[22] E. H. Hadi, D. A. Sabur, S. S. Chiad, N. F. Habubi, K., Abass, Journal of Green Engineering, 10 (10), 8390-8400 (2020); https://doi.org/10.1063/5.0095169
[23] D. M. A. Latif, S. S. Chiad, M. S. Erhayief, K. H. Abass, N. F. Habubi, H. A. Hussin, Journal of Physics, Conference Series 1003(1) 012108 (2018);
https://doi.org/10.1088/1742-6596/1003/1/012108
[24] M. D. Sakhil, Z. M. Shaban, K. S. Sharba, N. F. Habub, K. H. Abass, S. S. Chiad, A. S. Alkelaby, NeuroQuantology, 18 (5), 56-61 (2020);
https://doi.org/10.14704/nq.2020.18.5.NQ20168
[25] A. J. Ghazai, O. M. Abdulmunem, K. Y. Qader, S. S. Chiad, N. F. Habubi, AIP Conference Proceedings 2213 (1), 020101 (2020); https://doi.org/10.1063/5.0000158
[26] H. A. Hussin, R. S. Al-Hasnawy, R. I. Jasim, N. F. Habubi, S. S. Chiad, Journal of Green Engineering, 10(9)7018-7028 (2020); https://doi.org/10.1088/1742-6596/1999/1/012063
[27 E. S. Hassan, A. K. Elttayef, S. H. Mostafa, M. H. Salim and S. S. Chiad. Journal of aterials Science: Materials in Electronics, 30 (17),15943-15951 (2019);
https://doi.org/10.1155/2014/684317
[28] R. S. Ali, H. S. Rasheed, N. F. Habubi, S.S. Chiad, Lettersthis link is disabled, 20(1), 63–72 (2023; https://doi.org/10.15251/CL.2023.201.6
[29] M. S. Othman, K. A. Mishjil, H. G. Rashid, S. S. Chiad, N. F. Habubi, I. A. Al-Baidhany, Journal of Materials Science: Materials in Electronics, 31(11), 9037-9043 (2020);
https://doi.org/10.1007/s10854-020-03437-0
[30] B. J. Murray, Q. Li, J. T. Newberg, E. J. Menke, J. C. Hemminger and R. M. Penner, Chemistry of Materials, 17 (26) 6611-6618 (2005); http://dx.doi.org/10.1021/cm051647r
[31] B. J. Murray, J. T. Newberg, E. C. Walter, Q. Li, J. C. Hemminger and R. M. Penner, Analytical Chemistry, 77 (16) 5205-5214 (2005); http://dx.doi.org/10.1021/ac050636e
[32] E. Tselepis and E. Fortin, Journal of Materials Science, 21(3), 985-988 (1986);
http://dx.doi.org/10.1007/BF01117383
[33]A. A. Urabe, U. M. Nayef, R. Kamel, Journal of Science, 34(2),113-120 (2023);
DOI: http://doi.org/10.23851/mjs.v34i2.1223
[34] S. A. Hasan, J. A. Salman, S. S. Al-Jubori, Al-Mustansiriyah Journal of Science, 32(4), 21-25 (2021);
DOI: http://doi.org/10.23851/mjs.v32i4.1034
[35] k. H. Jebur, N. J. Mohammed, Al-Mustansiriyah Journal of Science, 32(4), 60-66 (2021);
DOI: http://doi.org/10.23851/mjs.v32i4.993
[36] B. E. Breyfogle, C. Hung, M. G. Shumsky and J. A. Switzer, Journal of the Electrochemical Society, 143 (9), 2741-2746 (1996);
http://dx.doi.org/10.1149/1.1837101
[37] H. T. Salloom, E. H. Hadi, N. F. Habubi, S. S. Chiad, M. Jadan, J. S. Addasi, Digest Journal of Nanomaterials and Biostructures, 15 (4), 189-1195 (2020);
https://doi.org/10.15251/DJNB.2020.154.1189
[38] R. S. Ali, M. K. Mohammed, A. A. Khadayeir, Z. M. Abood, N. F. Habubi and S. S. Chiad, Journal of Physics: Conference Series, 1664 (1), 012016 (2020);
https://doi:10.1088/1742-6596/1664/1/012016
[39] S. S. Chiad, H. A. Noor, O. M. Abdulmunem, N. F. Habubi, M. Jadan, J. S. Addasi, Journal of Ovonic Research, 16 (1), 35-40 (2020).
[40] N. N. Jandow, M. S. Othman, N. F.Habubi, S. S. Chiad, K. A. Mishjil, I. A. Al-Baidhany, Materials Research Express, 6 (11), (2020); https://doi.org/10.1088/2053-1591/ab4af8
[41] E. S. Hassan, K. Y. Qader, E. H. Hadi, S. S. Chiad, N. F. Habubi, K. H. Abass, Nano Biomedicine and Engineering, 12(3), pp. 205-213 (2020);
https://doi.org/10.5101/nbe.v12i3.p205-213

[42] R. S Ali, N. A. H. Al Aaraji, E. H. Hadi, N. F. Habubi, S. S. Chiad, Journal of Nanostructuresthis link is disabled, 10(4), 810–816 (2020); https://doi: 10.22052/jns.2020.04.014
[43] N. Y. Ahmed, B. A. Bader, M. Y. Slewa, N. F. Habubi, S. S. Chiad, NeuroQuantology, 18(6), 55-60 (2020); https://doi.org/10.14704/nq.2020.18.6.NQ20183
[44] A. A. Khadayeir, R. I. Jasim, S. H. Jumaah, N. F, Habubi, S. S. Chiad, Journal of Physics: Conference Series,1664 (1) (2020); https://doi.org/10.1088/1742-6596/1664/1/012009
[45] E. S. Hassan, T. H. Mubarak, K.H. Abass, S. S. Chiad, N. F. Habubi, M. H. Rahid, A. A. Khadayeir, M. O. Dawod, I. A. Al-Baidhany, Journal of Physics: Conference Series, 1234(1), 012013 (2019); https://doi.org/10.1088/1742-6596/1234/1/012013
[46] R. S. Ali, K. S. Sharba, A. M. Jabbar, S. S. Chiad, K. H. Abass, N. F. Habubi, NeuroQuantology 18 (1) 26-31 (2020);
https://doi.org/10.14704/nq.2020.18.1.NQ20103
[47] A. Ghazai, K. Qader, N. F. Hbubi, S. S. Chiad, O. Abdulmunem, IOP Conference Series: Materials Science and Engineering, 870 (1), 012027 (2020);
https://doi.org/ 10.1088/1757-899X/870/1/012027
[48] S. M. Hou, M. Ouyang, H. F. Chen et al., Thin Solid Films, 315 (1-2), 322–326 (1998);
https://doi.org/10.1016/S0040-6090(97)00713-X
[49] J. Tominaga, D. Buchel, C. Mihalcea, T. Shime, T. Fukaya, MRS Proceedings, S 7 (3), 728 (2002); https://doi.org/10.1088/0953-8984/15/25/201